ARTICLE

Tricellulin Is a Tight-Junction Protein Necessary for Hearing

Saima Riazuddin, Zubair M. Ahmed, Alan S. Fanning, Ayala Lagziel, Shin-ichiro Kitajiri, Khushnooda Ramzan, Shaheen N. Khan, Parna Chattaraj, Penelope L. Friedman, James M. Anderson, Inna A. Belyantseva, Andrew Forge, Sheikh Riazuddin, and Thomas B. Friedman

The inner ear has fluid-filled compartments of different ionic compositions, including the endolymphatic and perilymphatic spaces of the organ of Corti; the separation from one another by epithelial barriers is required for normal hearing. *TRIC* encodes tricellulin, a recently discovered tight-junction (TJ) protein that contributes to the structure and function of tricellular contacts of neighboring cells in many epithelial tissues. We show that, in humans, four different recessive mutations of *TRIC* cause nonsyndromic deafness (DFNB49), a surprisingly limited phenotype, given the widespread tissue distribution of tricellulin in epithelial cells. In the inner ear, tricellulin is concentrated at the tricellular TJs in cochlear and vestibular epithelia, including the structurally complex and extensive junctions between supporting and hair cells. We also demonstrate that there are multiple alternatively spliced isoforms of *TRIC* in various tissues and that mutations of *TRIC* associated with hearing loss remove all or most of a conserved region in the cytosolic domain that binds to the cytosolic scaffolding protein ZO-1. A wild-type isoform of tricellulin, which lacks this conserved region, is unaffected by the mutant alleles and is hypothesized to be sufficient for structural and functional integrity of epithelial barriers outside the inner ear.

In the inner ear, the endolymphatic and perilymphatic spaces of the organ of Corti are fluid-filled compartments of differing ionic compositions. This strict compartmentalization is required for normal hearing[1,2] and is accomplished by the tight-type tight junctions (TJs) of the reticular lamina, which consists of a mosaic of supporting cells and sensory hair cells. The apical membranes of the sensory hair cells and supporting cells are interconnected by uniquely complex bicellular TJs (bTJs) that are characterized by several parallel strands at the upper part of the TJ and an extensive labyrinth of irregular TJ strands in the lower part.[3,4] Among the large variety of TJ proteins, two members of the claudin family have been shown to be necessary for the normal function of the inner ear. Mutations of claudin 14 cause deafness in humans (DFNB29 [MIM 605608 and 610153]) and mice,[5–7] whereas a claudin 11 knockout mouse is also deaf.[8,9]

In addition to the selective permeability of bTJs, which helps to maintain the distinct ionic composition of compartments separated by epithelial barriers, the passage of solutes and ions is also assumed to occur through the tricellular region,[10–12] which has a unique architecture at the point where three epithelial cells contact one another.[13] Tricellulin was recently described as one of the constituents of tricellular TJs (tTJs) and perhaps of bTJs of epithelial barriers in general.[13]

Elsewhere, we reported two Pakistani families segregating nonsyndromic hearing loss that was linked to markers on chromosome 5q12.3-q14.1, and we defined an 11-cM interval for the DFNB49 locus.[14] Here, we refined this interval to 2.4 Mb after ascertaining six additional DFNB49-affected families. Among the numerous candidates in this refined DFNB49 interval are two genes encoding TJ tetraspan proteins of epithelial cells: tricellulin and occludin.[13,15] After excluding *OCLN* and seven other genes in the DFNB49 interval, we found that mutant alleles of *TRIC,* which encodes tricellulin, cosegregate with nonsyndromic moderate-to-profound DFNB49. We also show that tricellulin is concentrated in tTJs of mammalian inner-ear epithelia, including the tricellular junctions of the reticular lamina of the organ of Corti.

Material and Methods

Subjects

Subjects were enrolled in this study after we obtained their written informed consent. Approval was obtained from the National Institute of Neurological Disorders and Stroke/National Institute on Deafness and Other Communication Disorders (NIDCD) Institutional Review Board (IRB) at the National Institutes of Health (NIH), Bethesda (protocol OH-93-N-016) and from the IRB at the National Centre of Excellence in Molecular Biology, Lahore, Pakistan (protocol FWA00001758).

Clinical Evaluation

A general physical examination of all the affected individuals was conducted. No other clinical problem was found to consis-

From the Section on Human Genetics, Laboratory of Molecular Genetics, National Institute on Deafness and Other Communication Disorders, National Institutes of Health (NIH), Rockville, MD (S.R.; Z.M.A.; A.L.; S.-i.K.; P.C.; I.A.B.; T.B.F.); Department of Cell and Molecular Physiology, University of North Carolina, Chapel Hill (A.S.F.; J.M.A.); National Centre of Excellence in Molecular Biology, University of the Punjab, Lahore, Pakistan (K.R.; S.N.K.; S.R.); Internal Medicine Consult Service, Hatfield Clinical Research Center, NIH, Bethesda (P.L.F.); and Centre for Auditory Research, University College London Ear Institute, University College London, London (A.F.)

Received August 28, 2006; accepted for publication October 4, 2006; electronically published October 31, 2006.

Address for correspondence and reprints: Dr. Thomas B. Friedman, Laboratory of Molecular Genetics, National Institute on Deafness and Other Communication Disorders, National Institutes of Health, 5 Research Court, Room 2A-19, Rockville, MD 20850. E-mail: friedman@nidcd.nih.gov

Am. J. Hum. Genet. 2006;79:1040–1051. 0002-9297/2006/7906-0006$15.00

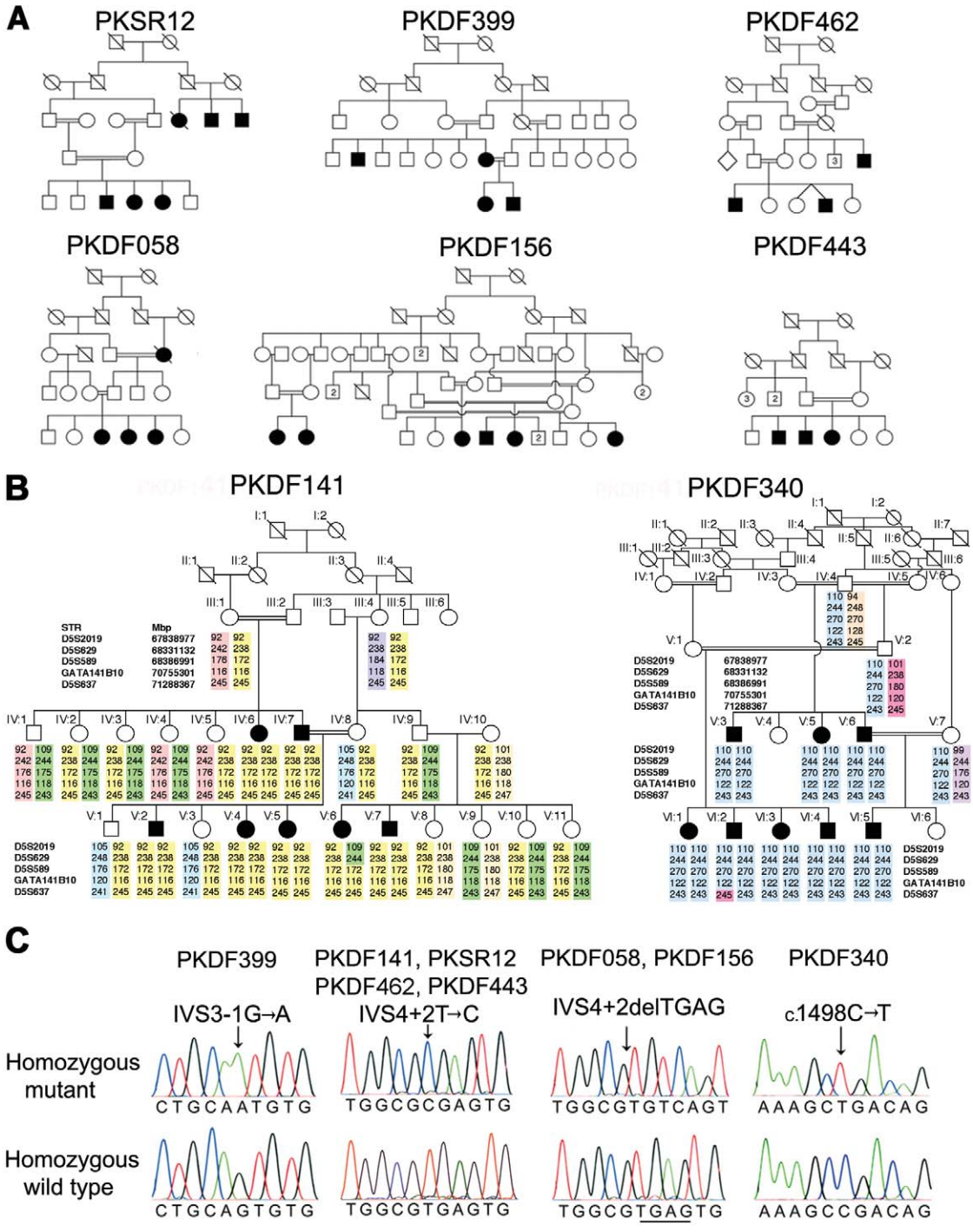

Figure 1. DFNB49-affected families segregating hearing loss associated with mutations of *TRIC*. *A,* Human pedigrees cosegregating hearing loss linked to markers in the DFNB49 interval. *B,* Haplotype of five STR markers linked to *TRIC* on chromosome 5 for families PKDF141 and PKDF340. Family PKDF141 has a maximum 2-point LOD score of 5.82 ($\theta = 0$) for marker *D5S589*. Individual IV:10 in family PKDF141 has the same disease haplotype and carries the same mutant allele of *TRIC* as does her spouse, suggesting common ancestry. Family PKDF340 has a maximum 2-point LOD score of 6.1 ($\theta = 0$) for *GATA141B10*. Meiotic recombinations define a linkage interval for DFNB49 between *D5S629* and *D5S637,* which, on a physical map, is from 68,311,260 to 71,336,684 bp (UCSC browser; May 2004 assembly). The proximal and distal breakpoints were identified in deaf individuals V:6 (PKDF141) and VI:2 (PKDF340), respectively. *C,* Representative sequence chromatograms of four mutations of *TRIC*.

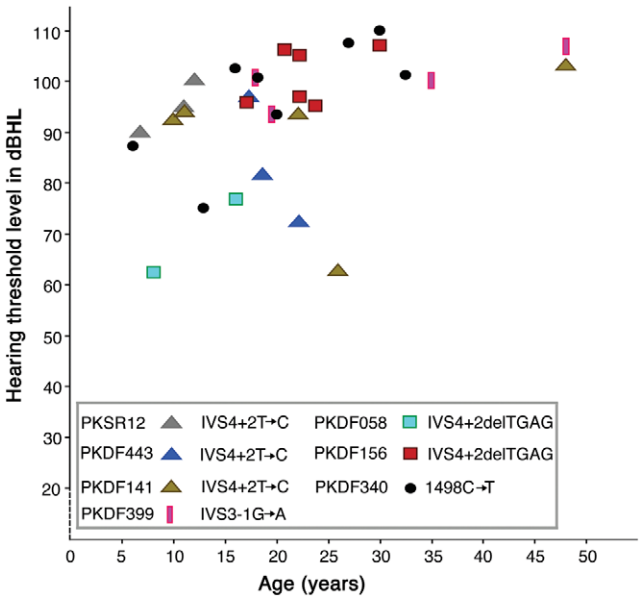

Figure 2. Pure-tone air-conduction averages (0.5, 1, 2, and 4 kHz) for the better-hearing ears of seven of the eight DFNB49-affected families. The *X*-axis is age, and the *Y*-axis is the average decibel (dBHL) at which the threshold of hearing is detected. There is inter- and intrafamilial variability in the severity of hearing loss due to recessive mutations of *TRIC,* which may be caused by genetic modifiers and/or environmental factors. For control subjects and normal-hearing members of families, hearing thresholds measured in ambient-noise conditions were 25–30 dBHL.

tently cosegregate with the hearing loss, including any vestibulopathy. An audiometric evaluation was performed on all of the affected individuals of the DFNB49-affected families by measuring the threshold of hearing at 250–8,000 Hz for pure-tone air conduction.

Sequencing

All DNA sequencing was performed using an ABI 3730 capillary instrument as described elsewhere.[16]

Generation and Growth of Lymphoblastoid Cell Lines

Lymphoblastoid cell cultures were established by the Coriell Institute, National Institute of General Medical Sciences Human Genetic Cell Project (NJ), through Epstein-Barr–virus transformation of peripheral-blood samples from deaf subjects and from controls. Cells were grown at 37°C in 5% CO_2 in RPMI-1640, supplemented with 1% of a 200-mM L-glutamine solution plus 15% fetal bovine serum (FBS) (heat inactivated).

RT-PCR with Use of RNA from Lymphoblastoid Cell Lines

Total RNA was isolated from cells by use of TRIzol reagent (Invitrogen). cDNA was synthesized with reagents from a SMART 1st strand cDNA synthesis kit (Clontech), and subsequent PCR reactions were performed with gene-specific primers designed from sequence in exons 2 and 6 (forward primer 5′-GGAGGACAGATAGCTGCAATG-3′; reverse primer 5′-TCATGGATTCTTGAAATTCTCTCA-3′). PCR fragments were subcloned into a TOPO cloning vector (Invitrogen), and the sequence was verified.

Exon Trapping

To determine the effect of the various mutant alleles of *TRIC* on RNA splicing, the wild-type and mutant alleles were PCR amplified from unaffected and deaf subjects, respectively, within 8.7 kb of genomic DNA encompassing exons 3, 4, and 5 (forward primer 5′-TCCGTATTCCCTACTCCTCTCTATG-3′; reverse primer 5′-GCCAGATTTTATTCATCCTCTAGATTT-3′). The three exons and 200 bp of flanking intronic sequence were verified for all constructs. For exon-trapping assays, we followed published protocols.[17,18] In brief, each of the constructs was transferred into pSPL3 (Gibco BRL [no longer commercially available]) and was transfected into COS-7 cells. Total RNA was isolated from these cells with use of TRIzol, and cDNA was synthesized. Nested vector primers were used, and the PCR fragments were subcloned and sequenced.

Freeze Fracture

The inner ears were removed from animals after decapitation, and cochleae were exposed. The oval and round windows were opened, and a small piece of bone was removed from the cochlear apex. Fixative (2.5% glutaraldehyde in 0.1 M cacodylate buffer with 3 mM $CaCl_2$) was gently injected into the inner ear through these openings, and the entire bulla was then immersed in fixative. Fixation continued for 1.5 h at room temperature, with gentle, slow rotation. Inner-ear tissue was dissected from the bulla and was incubated for at least 45 min in 25% glycerol before mounting on freeze-fracture planchettes and freezing in propane-isopentane (4:1) cooled in liquid nitrogen. Freeze fracture was performed in a Balzers BAF400D apparatus by use of standard procedures[19] and was viewed on a JEOL 1200EXII microscope. Digital images were adjusted in Photoshop 6.0 (Adobe) for optimal contrast and brightness.

Table 1. Family Data, Mutations of *TRIC,* and Allele Frequencies

Family	LOD at $\theta = 0$	Marker	Pathogenic *TRIC* Mutation
PKDF399	2.6	*D5S647*	IVS3-1G→A
PKDF058	2.4	*D5S647*	IVS4+2delTGAG
PKDF156	5.8	*GATA141B10*	IVS4+2delTGAG
PKDF141	5.8	*D5S589*	IVS4+2T→C
PKDF443	1.7	*D5S647*	IVS4+2T→C
PKDF462	1.7	*GATA141B10*	IVS4+2T→C
PKSR12	1.8	*D5S647*	IVS4+2T→C
PKDF340	6.1	*GATA141B10*	c.1498C→T p.R500X

NOTE.—Nucleotide changes are numbered according to the first coding ATG in exon 2 of *TRIC-a.* LOD scores were calculated using parameters described elsewhere.[26] Briefly, the disease was coded as fully penetrant, and the disease-allele frequency was set at 0.001. Meiotic recombination fractions were assumed to be equal for males and females. The three splice-site mutations of *TRIC* shown here were not found in at least 400 control chromosomes. See figure 3*C* and 3*D* for the predicted truncated tricellulin proteins resulting from each the three frameshifting splice-site mutations.

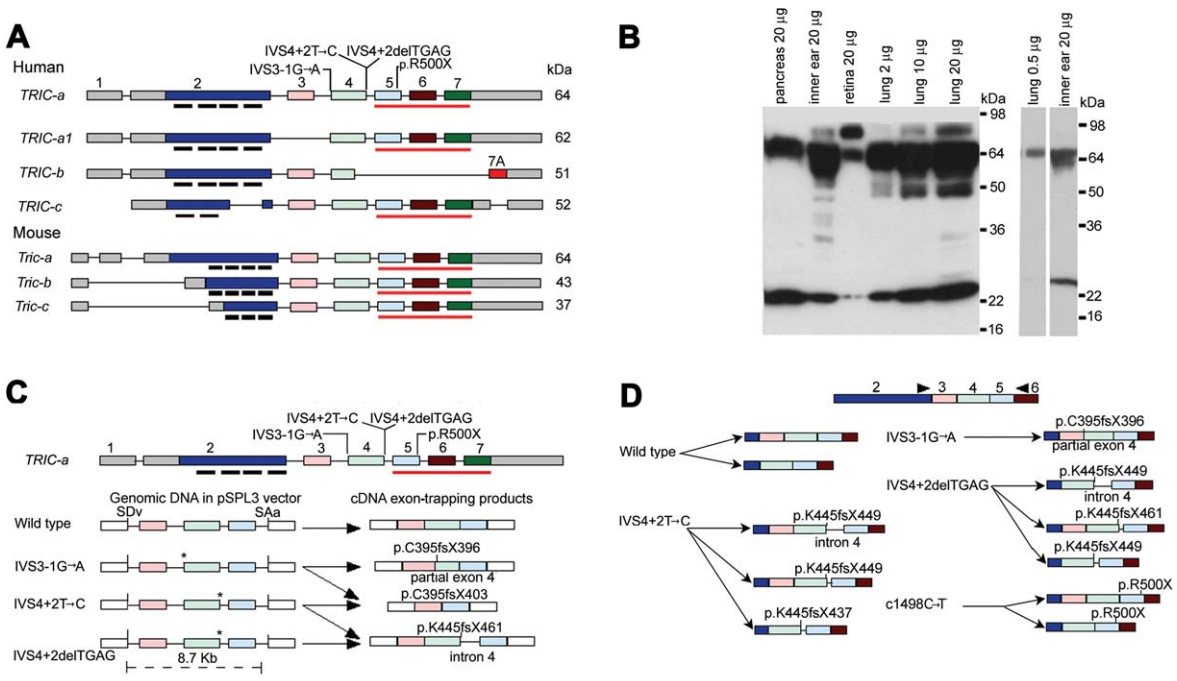

Figure 3. Wild-type isoforms of tricellulin, western-blot analysis, and aberrant RNA splice products that are due to mutant alleles of *TRIC*. *A,* Wild-type alternative splice isoforms of human *TRIC* and mouse *Tric*. Black bars under exon 2 show the position of the four predicted transmembrane helices. The red underline (also in panel C) indicates the occludin-ELL domain. The gray rectangles of exons 1 and 2 and of exon 7 are 5′ and 3′ UTRs, respectively. *B,* Western-blot analyses—through use of anti-tricellulin antibody HL5573 and protein extracts from adult C57BL/6J mouse pancreas, inner ear, retina, and lung—show a 64-kDa band in all lanes corresponding to a protein of the predicted size for *Tric-a*. In the retina, there is an abundant isoform of *TRIC* that is ~80 kDa, which is also present at a lower concentration in lung and inner ear. In protein from lung, there is a 64-kDa band, whereas there are two bands at ~64 kDa in protein from the cochlea. The right panel shows a western-blot analysis with a reduced amount of protein loaded on the gel for lung and a shorter exposure for the lane with protein from the cochlea. *C,* Aberrant splice products from exon-trapping assays. IVS3-1G→A causes the use of a cryptic splice-acceptor site within exon 4 of *TRIC,* which results in the deletion of the first 17 nt of exon 4 and a nonsense mutation (p.C395fsX396). IVS3-1G→A and IVS4+2T→C cause skipping of exon 4, which results in a frameshift and premature termination of translation (p.C395fsX403). IVS4+2delTGAG mRNA uses a cryptic splice-donor site in intron 4 that introduces 23 bp of intron 4, which results in a premature stop codon (p.K445fsX461). Locations of the mutant alleles are indicated by an asterisk (*). SDv and SAv are the splice-donor and splice-acceptor sites, respectively, encoded in vector sequence of pSPL3. *D,* Summary of RT-PCR data from lymphoblastoid cell lines of normal and (DFNB49) deaf individuals who have splice-site mutations of *TRIC*. The wild-type control showed the predicted splicing of exon 4 to exon 5 and alternative splicing of exon 3. mRNA isolated from lymphoblastoid cells from one deaf subject (each) of families PKDF399, PKDF443, PKDF058, and PKDF340 yielded aberrant splicing, and the locations of premature stop codons are indicated. Arrowheads indicate the locations of RT-PCR primers.

Antibodies

Tricellulin antiserum (PB705) was raised in rabbit against a synthetic peptide that is conserved in mice and humans (corresponding to residues 119–135 of the mouse sequence [GenBank accession number DQ682659]). Antiserum was affinity purified (AminoLink Plus Immobilization Kit [Pierce]), with the synthetic peptide used as the immunogen. In addition, antiserum (HL5573) to amino acids encoded by mouse exons 3 and 4 (residues 212–282 [GenBank accession number DQ682659]) was generated as a glutathione S-transferase (GST)–fusion protein. The cDNA was cloned into pGEX5.1 (Amersham Biosciences), was expressed in *Escherichia coli* (BL21GoldDE3pLysS [Stratagene]), was purified as described elsewhere,[20] and was injected into rabbits (Covance). To affinity purify antiserum HL5573, the sequence encoding the same amino acid residues was cloned into pMAL-c2x (New England Biolabs), transformed into *E. coli* Rosetta DE3 (Novagen), and the expressed protein was purified on amylose resin.[21] A column of MBP-tricellulin (residues 212–282) bound to 4% beaded agarose (Amino-Link Plus) was then used to affinity purify rabbit antisera HL5573. Fluorescein-conjugated mouse anti-occludin antibody and nonconjugated anti-mouse ZO-1 antibody were obtained from Zymed (Carlsbad), and fluorescein-conjugated anti-rabbit IgG secondary antibody was obtained from Amersham Pharmacia Biotech.

Specificity of Antibodies

Antibody specificity was validated by transfections (Lipofectamine-2000 [Life Technologies]) of GFP-tagged tricellulin into HeLa cells, followed by immunostaining with PB705 and HL5573 antisera. *TRIC-a* was subcloned into a pEGFP-C2 vector (Clontech).

Figure 4. Alignment of human tricellulin encoded by *TRIC-a* and *TRIC-b* and tricellulin orthologs from five vertebrates. Black and red bars indicate the predicted transmembrane helices and occludin-ELL domain, respectively. There is no significant amino acid–sequence similarity between *TRIC* (formerly referred to as "*MARVELD2*") and *MARVELD1* or *MARVELD3* on chromosomes 10 and 16, respectively.

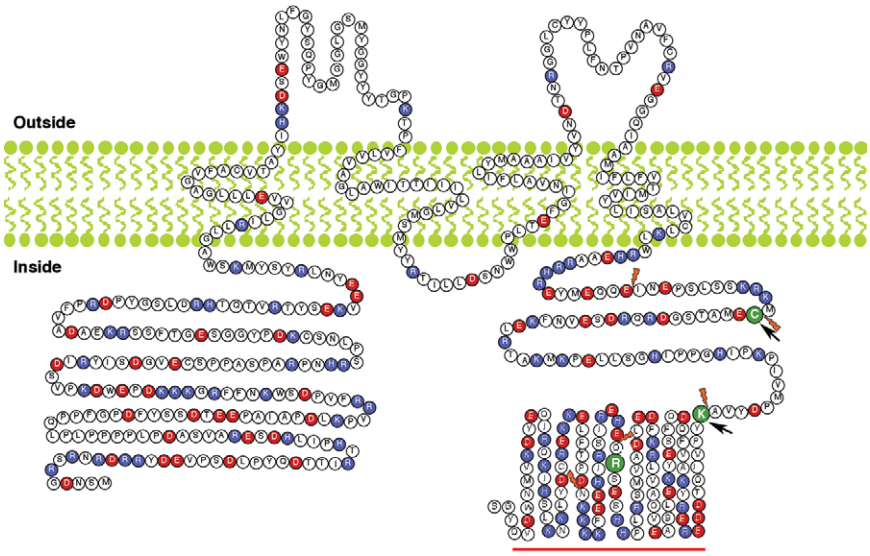

Figure 5. The predicted protein structure of *TRIC-a,* the longest isoform encoded by *TRIC*. Topology of the tricellulin was predicted by TMpred software. Of the 37 residues, 15 (40.5%) in the first extracellular loop are glycine and tyrosine. Red and blue amino acids indicate negatively and positively charged residues, respectively. The N- and C-termini consist of 31.6% and 41.4% charged residues, respectively. The position of an arginine codon mutated in family PKDF340 (p.R500X) is shown as a green R. Orange daggers indicate boundaries of the six coding exons of *TRIC*. Arrows indicate the locations of translation frameshifts due to splice-acceptor mutation (IVS3-1G→A) and splice-donor mutations (IVS4+2T→C and IVS4+2delTGAG), which occur at codons for residues C395 and K445, respectively. The red bar indicates the occludin-ELL domain.

HeLa cells were cultured in 10% FBS-supplemented Dulbecco's modified Eagle's medium. Fluorescence immunocytochemistry was performed on fixed cells (4% paraformaldehyde, for 15 min). Immunoflourescence staining with PB705 and HL5573 antibodies overlapped with the signal produced by GFP-tagged tricellulin expressed in HeLa cells (data not shown).

Western-Blot Analysis

C57BL/6J mouse pancreas, inner ear, retina, and lung were sonicated in an ice-cold PBS containing protease inhibitor (Calbiochem). Proteins were extracted and denatured by boiling for 5 min in SDS-PAGE sample buffer (0.125 M Tris-HCl, 20% glycerol, 4% SDS, and 0.005% Bromo-phenol blue). A 20-μg protein sample was separated on a 4%–20% gradient Tris-glycine gel (Novex), was transferred to a polyvinylidene fluoride (PVDF) membrane, was blocked overnight with 5% dry milk in tris-buffered saline with Tween (10 mM Tris-HCl [pH 7.5], 150 mM NaCl, and 0.05% Tween 20), and was stained with anti-tricellulin antiserum (HL5573; 1:2,000 in blocking solution) for 2 h at room temperature. After three washes, the membranes were incubated in a 1:5,000 dilution of horseradish peroxidase–conjugated anti-rabbit secondary antibody (Promega) for 30 min and were developed using the ECL Plus western-blotting detection system (Amersham Pharmacia Biotech).

Immunostaining

Temporal bones were dissected from C57BL/6 mice, the perilymphatic space was gently perfused with 10% trichloroacetic acid (TCA) through the round to the oval window, and samples were immersed in 10% TCA for 45 min at 4°C and were washed 3 times with PBS.[2] Tissue was then treated with 0.2% Triton X-100 in PBS for 15 min and was soaked in 1% BSA in PBS. The specimens were incubated overnight with primary antibodies at 4°C and then were washed three times with PBS, followed by a 30-min incubation with Alexa Fluor 594– or Alexa Fluor 488–conjugated secondary antibody. After several washes with PBS, tissue was mounted using ProLong Antifade (Molecular Probes) and was observed with a confocal microscope (LSM 510 META [Carl Zeiss MicroImaging]).

Purification of GST-Fusion Protein for Binding Assay

GST-fusion proteins encoding human occludin amino acid residues 371–522 (GST-hDOC$_{371–522}$), occludin with a point mutation (hDOC K433D) that abrogates ZO-1 binding, or the entire C-terminal cytosolic domain of different tricellulin isoforms were expressed in *E. coli* BL21 (pLys) and were purified on glutathione-agarose as described elsewhere.[22] All fusion proteins were clarified at 100,000 *g* immediately before use, and concentrations were calculated from the absorbance at A_{280}.

Purification of ZO1-N from Insect Cells

High Five cells (Invitrogen) were infected with a bacmid produced from the pFastBacHTa expression vector encoding amino acids 1–888 of human ZO-1 (ZO1-N [Genbank accession number AAA02891]). Cells were harvested 2 d after infection and were frozen at −80°C. To purify the recombinant ZO-1, infected cells were lysed in 6 volumes of Lysis Buffer (20 mM Tris-Cl [pH 8], 500 mM NaCl, 10% glycerol, 0.8% Igepal CA-630, 12.5 mM imidazole, 5 mM 2-mercaptoethanol, and Complete Protease Inhibitor Cocktail [Roche Applied Science]), were homogenized with

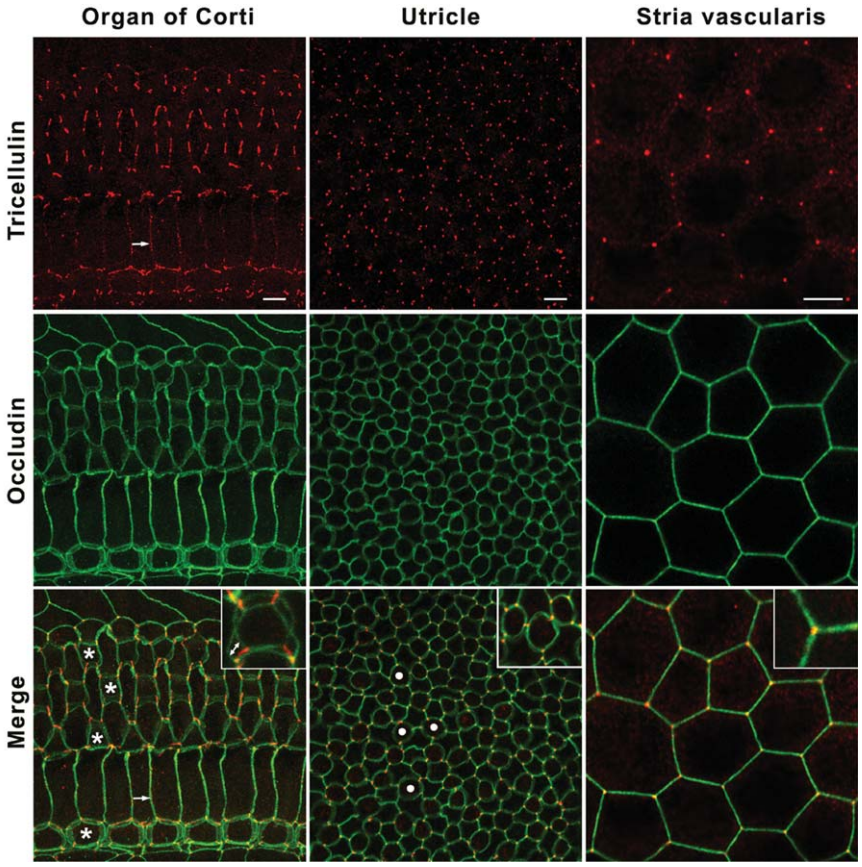

Figure 6. Immunofluorescence confocal images from P16 mouse inner-ear epithelia stained with anti-tricellulin pAb PB705 (*red*) and anti-occludin FITC-conjugated antibody (*green*) or mouse anti-ZO-1 mAb (*shown in the insets* [*green*]). The left panels represent a flattened stack of optical z-sections through the cuticular plates of organ-of-Corti hair cells. The middle panels represent an optical section at the top of round-shaped cuticular plates of vestibular hair cells (*white dots*) that are surrounded by polygonally shaped apical portions of supporting cells. The right panels represent an optical section through the apical plasma membrane of the polygonally shaped marginal cells of the stria vascularis. In the organ of Corti, there are three rows of outer hair cells and one row of inner hair cells (indicated by an asterisk [*] [*left panel*]) surrounded by supporting cells. Tricellulin is concentrated at contact points where three occludin-positive TJs converge in epithelial cells from the organ of Corti (*left panels*), in vestibular epithelia of the utricle (*middle panels*), and in marginal cells of the stria vascularis (*right panels*). Fainter staining for tricellulin is seen at bTJs (*arrow* [*left panel*]). In hair cells of the organ of Corti, occludin (*left panel*) and ZO-1 (*insets* [*left panel*] and video 1 [online only]) staining intersect tricellulin at the apical and basal ends of the tricellular junction, which extends downward from the apical surface and spans the entire depth of the hair-cell cuticular plate (*double-headed arrow*). In the vestibular epithelia and stria vascularis, tricellulin appears to be colocalized also with ZO-1 at the apical end of the tricellular junctions (*insets* [*middle and left panels*]). Scale bars = 5 μm.

20 strokes of a dounce homogenizer, and were centrifuged at 4°C for 10 min at 20,000 *g*. The soluble supernatant was combined with HIS-Select HF Nickel Affinity Gel (25 μl resin/ml lysate) and was incubated for 30 min at 4°C. Beads were washed twice in 20 volumes of Buffer I (20 mM Tris-Cl [pH 8], 200 mM NaCl, 10% glycerol, 0.2% Igepal CA-630, 12.5 mM imidazole, and 5 mM 2-mercaptoethanol), twice in Buffer II (20 mM Tris-Cl [pH 8], 100 mM NaCl, 10% glycerol, 0.5% Igepal CA-630, 12.5 mM imidazole, and 5 mM 2-mercaptoethanol), and received a final wash in binding buffer (PBS with 10% glycerol, 12.5 mM imidazole, and 5 mM 2-mercaptoethanol). The concentration of protein on the beads was estimated by eluting protein in 125 mM imidazole from a known quantity of beads and measuring the A_{280} of the eluate.

Tricellulin-Binding Assays

ZO1-N immobilized on agarose (0.5 μM) or agarose beads alone were mixed with 5.0 μM of the respective GST-fusion protein in a final volume of 0.5 ml and were incubated overnight at 4°C. The beads were washed four times in binding buffer, and the bound proteins were eluted in 100 μl of PBS containing 125 mM imidazole. The eluate was diluted in 100 μl sample buffer, was resolved by SDS-PAGE, and was stained with Coomassie Brilliant Blue.[23] Destained gels were scanned with an Odyssey Infrared Imaging System (LI-COR Biosciences).

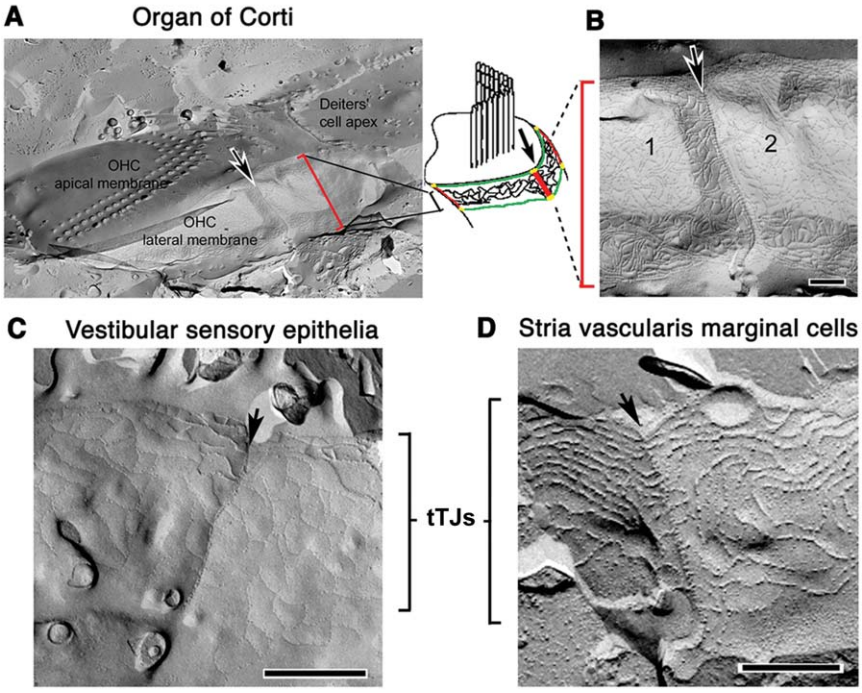

Figure 7. Freeze-fracture images of inner ear tTJs. *A,* At the apical end of an outer hair cell (OHC) in the organ of Corti of an adult guinea pig, the fracture has run across the apical membrane, cross-fracturing the bases of the stereocilia in the W-shaped bundle. At the border of the outer hair cell, where it would have contacted supporting cells, the fracture runs at 90° to the apical surface. The fracture exposes the whole depth of the hair cell tTJ down the lateral plasma membrane (*arrow*). The drawing shows TJ strands at the level of the most apical part of the lateral membrane (vertical red bars indicate the length of the tTJ; green lines represent ZO-1 staining outlining the cuticular plate at the top and bottom) (see fig. 6 [left panels]). *B,* The tTJ (*arrow*) at the site of contact of an outer hair cell with two supporting cells (1 and 2) is a distinct ridge from which short strands extend zipperlike to either side. *C,* For the mouse utricular macula, tTJs are less complex than those of an outer hair cell but also appear zipperlike. *D,* For the marginal cells of the stria vascularis, the tTJs appear similar to those of conventional epithelial cells such as Eph4 cells.[13] Scale bars = 5 μm.

Results

Elsewhere, we reported two Pakistani families segregating moderate-to-profound hearing loss consistent with linkage to *DFNB49*[14] (figs. 1*A* and 2). Meiotic information from six additional families refined the disease-linked haplotype to 2.4 Mb (fig. 1*B*). This interval has 33 annotated genes. We sequenced the reported exons of nine genes—*TRIC,* which encodes tricellulin[13] (formerly referred to as "*MARVELD2*"), *OCLN,*[24,25] *GTF2H2, SMA3, SMA4, TAF9, RAD17, SLC30A5,* and *KENA*—using genomic DNA from two affected members of each of the eight DFNB49-affected families. We found pathogenic mutations only in *TRIC* (table 1). In humans, the longest *TRIC* mRNA (*TRIC-a*) has seven exons (GenBank accession number DQ682656), which are predicted to encode four transmembrane domains and an occludin-ELL domain (Pfam accession number PF07303) located at the C-terminus (fig. 3*A*).

Affected individuals from families PKDF141, PKSR12, PKDF462, and PKDF443 (fig. 1*A* and 1*B*) are homozygous for the same disease haplotype and have the same transition mutation—*TRIC* (IVS4+2T→C)—located in the splice-donor site of exon 4 of *TRIC* (fig. 1*C*). Families PKDF058 and PKDF156 segregate a deletion (IVS4+2delTGAG) of this same splice-donor site, and family PKDF399 segregates a mutation in the splice-acceptor site of exon 4 (IVS3-1G→A). Affected members of family PKDF340 are homozygous for a transition mutation (c.1498C→T) that creates a nonsense codon, p.R500X, in exon 5 of *TRIC,* which predicts a truncation within the occludin-ELL domain (fig. 1*C*). All of these recessive mutations of *TRIC* cosegregate with hearing loss in the families. None of these mutations were detected in a total of 443 normal-hearing subjects from Pakistan (n = 263), India (n = 90), and the Human Variation Panel (n = 90) (Coriell Cell Repositories) (table 1).

The longest isoform of *TRIC* is *TRIC-a,* which we detected in human fetal cochlear mRNA by RT-PCR. *TRIC-a* is predicted to encode a protein of 558 aa, whereas the *TRIC-a1* (GenBank accession number DQ682657) message lacks exon 3 (figs. 3*A,* 4, and 5). At the C-terminus of the

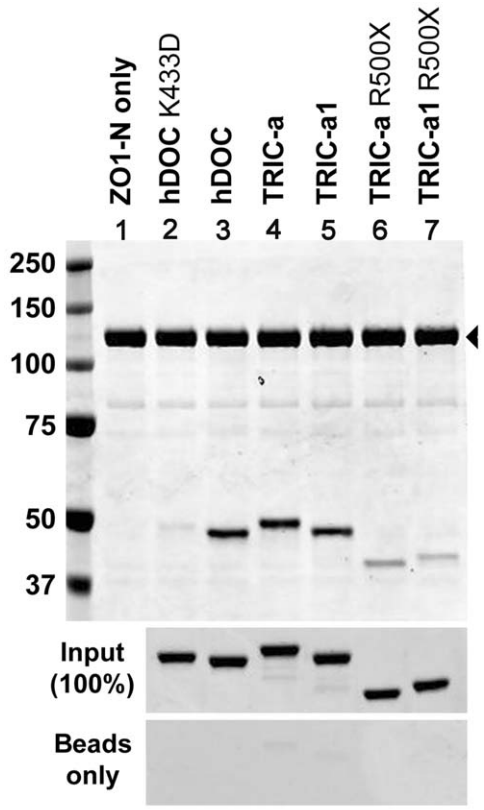

Figure 8. The binding of tricellulin to ZO-1, disrupted in p.R500X-truncated tricellulin. Proteins were resolved by SDS-PAGE and were stained with Coomassie Brilliant Blue. *Top panel, lane 1,* Control has only the N-terminal half of ZO-1 immobilized on agarose beads (ZO1-N; amino acids 1–888). *Lanes 2 and 3,* GST-fusion proteins encoding the corresponding domains of hDOC (amino acids 371–522) and a mutant occludin (hDOC K433D) that cannot bind to ZO1-N, used as positive and negative controls, respectively.[15] *Lanes 4–7,* GST-fusion proteins encoding TRIC-a and TRIC-a1 bind ZO1-N, whereas truncated tricellulin, because of p.R500X, has reduced binding to ZO1-N. Compare lanes 4 and 5 with lanes 6 and 7. The purified ZO1-N fusion protein (*arrowhead*) was also resolved for comparison; there is little, if any, degradation of fusion proteins detected after binding. *Middle panel,* Purified GST-fusion proteins carried through the binding assay without ZO1-N. *Bottom panel,* Little or no binding of fusion proteins to agarose alone. The molecular weight markers are shown in kilodaltons.

TRIC-a and *TRIC-a1* isoforms, there is a 103-aa residue occludin-ELL domain that is 32% identical (51% similar) to a region of the C-terminus of occludin. In contrast, *TRIC-b* is a shorter isoform (GenBank accession number NM144724) that was reported to be cloned from human lung, mammary gland, and eye mRNA and encodes 458 aa lacking the occludin-ELL domain (fig. 3*A*). *TRIC-c* (GenBank accession number DQ682658), which encodes 442 aa, was cloned from mRNA isolated from human lung. In this isoform, exon 2 is alternatively spliced and encodes only two predicted transmembrane helices (fig. 3*A*). From RNA isolated from the mouse cochlea, similar isoforms of tricellulin were found (*Tric-a, Tric-b,* and *Tric-c* [GenBank accession numbers DQ682659, DQ682660, and DQ682661, respectively). Western-blot analyses of proteins isolated from various mouse tissues show the expected size bands corresponding to tricellulin isoforms (fig. 3*B*).

Exon-trapping assays were performed to determine the effects of the three different splice-site mutations on *TRIC* mRNA processing. A wild-type *TRIC* construct produced the expected splice products (fig. 3*C*), whereas each of the splice-site mutant constructs produced only aberrantly spliced RNAs with premature stop codons (fig. 3*C*). To determine whether these or other aberrant splice variants occur in vivo, RNA was isolated from lymphoblastoid cell lines of affected subjects, each homozygous for one of the three splice-site mutations. RT-PCR analyses of transcripts from these lymphoblastoid cell lines resulted only in aberrantly spliced products (15 clones evaluated for each cell line), 2 of which were also found in the exon-trapping experiments (fig. 3*D*). By comparison, lymphoblastoid cells from a control subject with a wild-type sequence for *TRIC* produced wild-type isoforms of *TRIC* with and without alternatively spliced exon 3 (fig. 3*D*). mRNA for *TRIC* was also recovered from a lymphoblastoid cell line from a deaf individual who is homozygous for p.R500X; thus, at least some R500X mRNA escapes degradation by the nonsense-mediated decay pathway[27] (fig. 3*D*).

In postnatal day 5 (P5), P10, P16, and P90 mouse inner ears, which were counterstained with anti-occludin and ZO-1 antibodies, tricellulin was found to be concentrated at tricellular points of contact in the majority of epithelial cells of the cochlea and vestibule, and a weaker punctate signal was observed along the bTJs (fig. 6 and data not shown). At the junctions of outer hair cells with two adjacent supporting cells, we observed tricellulin immunoreactivity along the entire depth of tricellular junctions, extending in near-perpendicular orientation to the reticular lamina, as far down as the depth of the hair-cell cuticular plate (an actin-rich structure into which stereocilia rootlets are embedded) highlighted by the anti-occludin antibody (fig. 6). Tricellulin appears to intersect, at an ~90° angle, the perimeter of the two rings of ZO-1 that outline the top and the bottom of the cuticular plate (fig. 6 [insets in the left panel] and video 1 [online only]). Tricellulin immunoreactivity also spans the entire depth of tTJs of other epithelial cell types as well, although the tTJs of the nonsensory epithelium do not appear as deep as the tTJs of the sensory epithelium of the organ of Corti (fig. 6).

Freeze-fracture replica electron microscopy shows that, in the organ of Corti (fig. 7*A* and 7*B*), tricellular junctions have an elaborate structure, characterized by a long ridge resembling a zipper, oriented perpendicular to the apical surface (fig. 7). The tTJs of the vestibular sensory epithelium (fig. 7*C*), although relatively deep, are not as complex as those of hair cells of the organ of Corti. By comparison,

the tricellular junctions of the stria vascularis (fig. 7*D*) are not as deep and are similar to the central sealing elements of tTJs observed in cells derived from the mouse mammary gland (Eph4 cells) and other nonsensory epithelial cells.[13]

The C-terminal domain of occludin is known to bind the scaffolding protein ZO-1, which controls its targeting to the cell-cell junctions.[15] The high-resolution structure of this domain has been determined,[15] and sequence comparison with the occludin-ELL domain of tricellulin indicates that tricellulin contains all the structural elements and several specific surface residues required for binding to ZO-1. Therefore, we examined the ability of GST-fusion proteins encoding the cytosolic C-terminal domains of different tricellulin isoforms to bind in vitro to purified ZO-1. We found that wild-type tricellulin, like a C-terminal fragment of occludin containing the human occludin-ELL domain residues (hDOC), binds in vitro directly to the ZO-1 polypeptide. In contrast, binding of the p.R500X mutant tricellulin protein to ZO-1 was significantly compromised (fig. 8).

Discussion

Epithelial cell sheets separate fluid-filled compartments of polarized tissues. Within these sheets, intercellular junctional complexes composed of adherens junctions and desmosomes serve to mechanically link adjacent cells. TJs are continuous beltlike strands or fibrils[11,28] that encircle the cell near the apical surface and create a semipermeable paracellular seal.[29] TJs are composed of many proteins, including occludin[24,25] and one or more members of the large family of claudins.[30] Claudins are tetraspan integral membrane proteins that contribute to charge and size-selective pores of the paracellular barrier.[31–33] Both claudins and occludin are associated with one or more members of the MAGUK family of scaffolding proteins—including ZO-1, -2, and -3—and these interactions are important for the assembly of TJs.[34]

TRIC encodes tricellulin, a newly discovered TJ protein,[13] which is ubiquitously expressed in epithelial junctions of tissues and organs throughout the body. When tricellulin is down-regulated by RNAi (RNA interference), cells become electrophysiologically compromised and both the tTJs and bTJs are disorganized.[13] Yet the only obvious phenotype of mutant alleles of *TRIC* is deafness. It is possible that some other molecule compensates for the absence of wild-type tricellulin in other epithelial cell types but not in the inner ear. Alternatively, the exon 4 splice-site mutant alleles (IVS3-1G→A, IVS4+2T→C, and IVS4+2delTGAG) associated with deafness do produce, in vivo, a small amount of wild-type *TRIC* message and protein sufficient for tricellular-junction function in other epithelial cells but not in the inner ear. This seems unlikely, since we did not detect wild-type *TRIC* mRNA either in our exon-trapping experiments or in lymphoblastoid cell lines derived from affected individuals. A third possibility is that the wild-type short isoform of tricellulin (e.g., *TRIC-b*) may be present in many tissues and may be sufficiently functional for these tricellular junctions. However, *TRIC-b*–encoded protein should not bind ZO-1. Perhaps this binding activity is absolutely required for tTJs in the inner ear but not in other epithelia. A fourth possibility is that mutant, truncated tricellulin protein, if synthesized in vivo, provides a sufficiently tight barrier for intermediate-to-tight junctions in many epithelial tissues but is not able to maintain the unusually high tightness of the TJs of the organ of Corti.

A common feature of the four DFNB49 tricellulin alleles is that they encode predicted truncated proteins that lack the ability to bind to the scaffolding protein ZO-1, and probably to ZO-2 and ZO-3 as well, because of the loss of the conserved C-terminal occludin-ELL domain. Mutations in the same domain in occludin can interfere with the localization to TJs.[15] Thus, it is interesting to speculate that at least one underlying cause of cellular dysfunction in the cochlea is the inability to incorporate these mutant tricellulin proteins into the cytosolic scaffold formed by ZO proteins. Fanning and coauthors reported that ZO-1 can directly bind to F-actin–linking transmembrane proteins, such as occludin and claudins, to the actin cytoskeleton.[35] In this regard, the tTJs of hair cells may be attached intracellularly to cytoskeletal actin of the cuticular plate into which stereocilia rootlets are embedded. Therefore, a possible reason for the deafness phenotype due to mutations of *TRIC* is that the reticular lamina in the organ of Corti is less rigid, leading either to abnormalities in stereocilia microdeflections or to the inability of the reticular lamina to withstand the mechanical stress of outer hair–cell motility. These ideas can be tested in a mouse model of DFNB49, but elucidating the function of tricellulin in other tissues will require strategies that selectively and individually remove each of the tricellulin isoforms.

Dysfunction of endothelial or epithelial bTJ barriers is associated with a variety of inherited and neoplastic disorders,[5,6,836–42] as well as with pathological processes caused by certain infectious pathogens.[43] To date, mutant alleles of *TRIC* are the only known cause of compromised tricellular junctions of epithelial cells. Further study of tricellulin could help to provide a rational molecular framework useful for engineering novel therapeutic agents that could effectively target and modulate bTJs and tTJs.

Acknowledgments

We thank the members of the families for participation in our study. For critiques of our manuscript and ideas, we thank T. Ben-Yosef, R. Chadwick, D. Drayna, G. Frolenkov, A. Griffith, M. Kelley, R. Morell, S. Sullivan, J. Schultz, and J. Cyr. We thank D. Utepbergenov for technical advice and for providing the insect cell-expression system for ZO-1, and we acknowledge Z. Pasha for clinical evaluations. This study was supported by the Higher Education Commission, Islamabad, Pakistan, and the International Centre for Genetic Engineering and Biotechnology, Trieste, Italy (CRP/PAK02-01) (to S.R.); the Wellcome Trust (to A.F.); Na-

tional Institute of Diabetes and Digestive and Kidney Diseases grant DK61397 (to J.M.A. and A.S.F.); a research fellowship from the Japan Society for the Promotion of Science (to S.K.); and by intramural funds from NIDCD, NIH, grants ZO1 DC000035-08 and Z01 DC000039-08 (to T.B.F.).

Appendix A

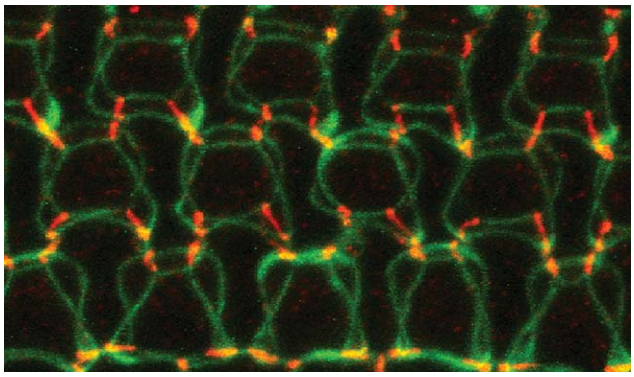

Video 1. The 3D reconstruction of the series of optical z-sections through the cuticular plates of organ of Corti outer hair cells. The video (a .MOV file [online only] that can be viewed with QuickTime [available at the Apple Web site]) shows three rows of outer hair cells surrounded by supporting cells. Tricellulin (*red*) is concentrated at contact points where three bTJs outlined by ZO-1 staining (*green*) converge in epithelial cells from the organ of Corti. ZO-1 (*green*) and occludin (shown in fig. 6) staining intersect tricellulin at the apical and basal end of the tricellular junction, which extends downward from the apical surface and spans the entire depth of the hair-cell cuticular plate. The 3D reconstruction was created using LSM510 software (Carl Zeiss MicroImaging).

Web Resources

Accession numbers and URLs for data presented herein are as follows:

Apple, http://www.apple.com/quicktime/download/win.html (for QuickTime download)

GenBank, http://www.ncbi.nlm.nih.gov/Genbank/ (for residues 119–135 [accession number DQ682659] and 212–282 [accession number DQ682659], ZO1-N [accession number AAA02891], and exons for *TRIC-a* [accession number DQ682656], *TRIC-a1* [accession number DQ682657], *TRIC-b* [accession number NM144724], *TRIC-c* [accession number DQ682658], *Tric-a* [accession number DQ682659], *Tric-b* [accession number DQ682660], and *Tric-c* [accession number DQ682661])

Online Mendelian Inheritance in Man (OMIM), http://www.ncbi.nlm.nih.gov/Omim/ (for DFNB29)

Pfam, http://www.sanger.ac.uk/Software/Pfam/ (for occludin-ELL [accession number PF07303])

References

1. Sterkers O, Ferrary E, Amiel C (1988) Production of inner ear fluids. Physiol Rev 68:1083–1128
2. Kitajiri S, Furuse M, Morita K, Saishin-Kiuchi Y, Kido H, Ito J, Tsukita S (2004) Expression patterns of claudins, tight junction adhesion molecules, in the inner ear. Hear Res 187:25–34
3. Jahnke K (1975) The fine structure of freeze-fractured intercellular junctions in the guinea pig inner ear. Acta Otolaryngol Suppl 336:1–40
4. Gulley RL, Reese TS (1976) Intercellular junctions in the reticular lamina of the organ of Corti. J Neurocytol 5:479–507
5. Wilcox ER, Burton QL, Naz S, Riazuddin S, Smith TN, Ploplis B, Belyantseva I, Ben-Yosef T, Liburd NA, Morell RJ, Kachar B, Wu DK, Griffith AJ, Riazuddin S, Friedman TB (2001) Mutations in the gene encoding tight junction claudin-14 cause autosomal recessive deafness DFNB29. Cell 104:165–172
6. Ben-Yosef T, Belyantseva IA, Saunders TL, Hughes ED, Kawamoto K, Van Itallie CM, Beyer LA, Halsey K, Gardner DJ, Wilcox ER, Rasmussen J, Anderson JM, Dolan DF, Forge A, Raphael Y, Camper SA, Friedman TB (2003) Claudin 14 knockout mice, a model for autosomal recessive deafness DFNB29, are deaf due to cochlear hair cell degeneration. Hum Mol Genet 12:2049–2061
7. Morton CC, Nance WE (2006) Newborn hearing screening—a silent revolution. N Engl J Med 354:2151–2164
8. Gow A, Davies C, Southwood CM, Frolenkov G, Chrustowski M, Ng L, Yamauchi D, Marcus DC, Kachar B (2004) Deafness in claudin 11-null mice reveals the critical contribution of basal cell tight junctions to stria vascularis function. J Neurosci 24:7051–7062
9. Kitajiri S, Miyamoto T, Mineharu A, Sonoda N, Furuse K, Hata M, Sasaki H, Mori Y, Kubota T, Ito J, Furuse M, Tsukita S (2004) Compartmentalization established by claudin-11-based tight junctions in stria vascularis is required for hearing through generation of endocochlear potential. J Cell Sci 117:5087–5096
10. Staehelin LA (1974) Structure and function of intercellular junctions. Int Rev Cytol 39:191–283
11. Walker DC, MacKenzie A, Hulbert WC, Hogg JC (1985) A reassessment of the tricellular region of epithelial cell tight junctions in trachea of guinea pig. Acta Anat 122:35–38
12. Walker DC, MacKenzie A, Hosford S (1994) The structure of the tricellular region of endothelial tight junctions of pulmonary capillaries analyzed by freeze-fracture. Microvasc Res 48:259–281
13. Ikenouchi J, Furuse M, Furuse K, Sasaki H, Tsukit S, Tsukita S (2005) Tricellulin constitutes a novel barrier at tricellular contacts of epithelial cells. J Cell Biol 171:939–945
14. Ramzan K, Shaikh RS, Ahmad J, Khan SN, Riazuddin S, Ahmed ZM, Friedman TB, Wilcox ER, Riazuddin S (2005) A new locus for nonsyndromic deafness DFNB49 maps to chromosome 5q12.3-q14.1. Hum Genet 116:17–22
15. Li Y, Fanning AS, Anderson JM, Lavie A (2005) Structure of the conserved cytoplasmic C-terminal domain of occludin: identification of the ZO-1 binding surface. J Mol Biol 352:151–164
16. Ahmed ZM, Riazuddin S, Bernstein SL, Ahmed Z, Khan S, Griffith AJ, Morell RJ, Friedman TB, Riazuddin S, Wilcox ER (2001) Mutations of the protocadherin gene *PCDH15* cause Usher syndrome type 1F. Am J Hum Genet 69:25–34
17. Buckler AJ, Chang DD, Graw SL, Brook JD, Haber DA, Sharp PA, Housman DE (1991) Exon amplification: a strategy to isolate mammalian genes based on RNA splicing. Proc Natl Acad Sci USA 88:4005–4009
18. Ahmed ZM, Smith TN, Riazuddin S, Makishima T, Ghosh M,

Bokhari S, Menon PS, Deshmukh D, Griffith AJ, Riazuddin S, Friedman TB, Wilcox ER (2002) Nonsyndromic recessive deafness DFNB18 and Usher syndrome type IC are allelic mutations of USHIC. Hum Genet 110:527–531
19. Forge A, Davies S, Zajic G (1991) Assessment of ultrastructure in isolated cochlear hair cells using a procedure for rapid freezing before freeze-fracture and deep-etching. J Neurocytol 20: 471–484
20. Belyantseva IA, Boger ET, Naz S, Frolenkov GI, Seller JR, Ahmed ZM, Griffith AJ, Friedman TB (2005) Myosin-XVa is required for tip localization of whirlin and differential elongation of hair-cell stereocilia. Nat Cell Biol 7:148–156
21. Lagziel A, Ahmed ZM, Schultz JM, Morell JR, Belyanteseva IA, Friedman TB (2005) Spatiotemporal pattern and isoforms of cadherin 23 in wild type and waltzer mice during inner ear hair cell development. Dev Biol 280:295–306
22. Fanning AS, Jameson BJ, Jesaitis LA, Anderson JM (1998) The tight junction protein ZO-1 establishes a link between the transmembrane protein occludin and the actin cytoskeleton. J Biol Chem 273:29745–29753
23. Fairbanks G, Steck TL, Wallach DF (1971) Electrophoretic analysis of the major polypeptides of the human erythrocyte membrane. Biochemistry 10:2606–2617
24. Feldman GJ, Mullin JM, Ryan MP (2005) Occludin: structure, function and regulation. Adv Drug Deliv Rev 57:883–917
25. Furuse M, Hirase T, Itoh M, Nagafuchi A, Yonemura S, Tsukita S, Tsukita S (1993) Occludin: a novel integral membrane protein localizing at tight junctions. J Cell Biol 123:1777–1788
26. Schaffer AA (1996) Faster linkage analysis computations for pedigrees with loops or unused alleles. Hum Hered 46:226–235
27. Maquat LE (2004) Nonsense-mediated mRNA decay: splicing, translation and mRNP dynamics. Nat Rev Mol Cell Biol 5:89–99
28. Pinto da Silva P, Kachar B (1982) On tight-junction structure. Cell 28:441–450
29. Farquhar MG, Palade GE (1963) Junctional complexes in various epithelia. J Cell Biol 17:375–412
30. Turksen K, Troy TC (2004) Barriers built on claudins. J Cell Sci 117:2435–2447
31. Van Itallie CM, Anderson JM (2006) Claudins and epithelial paracellular transport. Annu Rev Physiol 68:403–429
32. Knust E, Bossinger O (2002) Composition and formation of intercellular junctions in epithelial cells. Science 298:1955–1959
33. Van Itallie CM, Anderson JM (2004) The molecular physiology of tight junction pores. Physiology 19:331–338
34. Gonzalez-Mariscal L, Betanzos A, Avila-Flores A (2000) MAGUK proteins: structure and role in the tight junction. Semin Cell Dev Biol 11:315–324
35. Fanning AS, Ma TY, Anderson JM (2002) Isolation and functional characterization of the actin binding region in the tight junction protein ZO-1. FASEB J 16:1835–1837
36. Weber S, Schlingmann KP, Peters M, Nejsum LN, Nielsen S, Engel H, Grzeschik KH, Seyberth HW, Grone HJ, Nusing R, Konrad M (2001) Primary gene structure and expression studies of rodent paracellin-1. J Am Soc Nephrol 12:2664–2672
37. Carlton VE, Harris BZ, Puffenberger EG, Batta AK, Knisely AS, Robinson DL, Strauss KA, Shneider BL, Lim WA, Salen G, Morton DH, Bull LN (2003) Complex inheritance of familial hypercholanemia with associated mutations in TJP2 and BAAT. Nat Genet 34:91–96
38. Simon DB, Lu Y, Choate KA, Velazquez H, Al-Sabban E, Praga M, Casari G, Bettinelli A, Colussi G, Rodriguez-Soriano J, McCredie D, Milford D, Sanjad S, Lifton RP (1999) Paracellin-1, a renal tight junction protein required for paracellular Mg^{2+} resorption. Science 285:103–106
39. Notterpek L, Roux KJ, Amici SA, Yazdanpour A, Rahner C, Fletcher BS (2001) Peripheral myelin protein 22 is a constituent of intercellular junctions in epithelia. Proc Natl Acad Sci USA 98:14404–14409
40. Kovach MJ, Lin J-P, Boyadjiev S, Campbell K, Mazzeo L, Herman K, Rimer LA, Frank W, Llewellyn B, Jabs EW, Gelber D, Kimonis VE (1999) A unique point mutation in the *PMP22* gene is associated with Charcot-Marie-Tooth disease and deafness. Am J Hum Genet 64:1580–1593
41. Harhaj NS, Antonetti DA (2004) Regulation of tight junctions and loss of barrier function in pathophysiology. Int J Biochem Cell Biol 36:1206–1237
42. Mullin JM, Agostino N, Rendon-Huerta E, Thornton JJ (2005) Epithelial and endothelial barriers in human disease. Drug Discov Today 10:395–408
43. Sears CL (2000) Molecular physiology and pathophysiology of tight junctions V: assault of the tight junction by enteric pathogens. Am J Physiol Gastrointest Liver Physiol 279:G1129–G1134